Available online at www.sciencedirect.com
ScienceDirect
Infrared Physics & Technology 50 (2007) 136–141
INFRARED PHYSICS & TECHNOLOGY
www.elsevier.com/locate/infrared

Band structure and impurity effects on optical properties of quantum well and quantum dot infrared photodetectors

D.Z.-Y. Ting [a,*], Y.-C. Chang [b], S.V. Bandara [a], C.J. Hill [a], S.D. Gunapala [a]

[a] Jet Propulsion Laboratory, California Institute of Technology, Pasadena, CA 91109, USA
[b] Department of Physics, University of Illinois at Urbana-Champaign, Urbana, IL 61801, USA

Available online 6 December 2006

Abstract

We examined theoretically band structure and discrete dopant effects in the quantum well infrared photodetector (QWIP) and the quantum dot infrared photodetector (QDIP). We find that in QWIPs discrete dopant effects can induce long wavelength infrared absorption through impurity assisted intra-subband optical transitions. In QDIPs, we find that a strategically placed dopant atom in a quantum dot can easily destroy the symmetry and modify the selection rule. This mechanism could be partially responsible for normal incidence absorption observed in low-aspect-ratio quantum dots.

Keywords: Infrared; Quantum well; Quantum dot; QWIP; QDIP; Discrete dopant effect

1. Introduction

It has been predicted that quantum dot infrared photodetectors (QDIPs) with high dot densities and uniformity could outperform quantum well infrared photodetectors (QWIPs) [1,2], in part due to their normal incidence absorption properties. However, in the typical InAs/GaAs QDIP, the dots are much wider in the base than they are tall. In such low-aspect-ratio dots, while the ground to the first excited state transition can produce strong normal incidence absorption, it does not contribute appreciably to the photocurrent under small or moderate biasing conditions because the first excited state is deeply bound. Instead, the typical observed photo-response is due to transition to higher excited states. Experimentally, we found QDIP normal incidence absorption to be several times weaker than absorption of light polarized in the growth direction, but significantly stronger than that found in QWIPs. One possible explanation of the size of the normal incidence absorption is band structure effect. In QWIPs, non-zero (though rather small) normal incidence absorption is permitted when band mixing is taken into account. In this paper we model QDIP optical properties using a non-parabolic effective mass equation that incorporate the contributions of the 14-band $k \cdot p$ model for inter-subband optical transitions. Another possibility is impurity effect. On the scale of a quantum dot, the dopant potential represents a significant perturbation. We therefore expect that a strategically placed dopant atom in a quantum dot can easily destroy the symmetry and modify the selection rule. We have implemented an efficient theoretical method which allows us to study discrete dopant effects. We apply our method to examine discrete dopant effects on the optical properties of quantum wells and quantum dots.

2. Theoretical method

We model the detector structure by solving the effective mass approximation (EMA) equation over a laterally repeating 3D supercell, illustrated in Fig. 1. The supercell is periodic in the x and y dimensions with periodicities L_x and L_y, respectively. Along the growth (z)-direction, an active region of thickness L_z is surrounded by the

* Corresponding author.
E-mail address: David.Z.Ting@jpl.nasa.gov (D.Z.-Y. Ting).

1350-4495/$ - see front matter © 2006 Elsevier B.V. All rights reserved.
doi:10.1016/j.infrared.2006.10.031

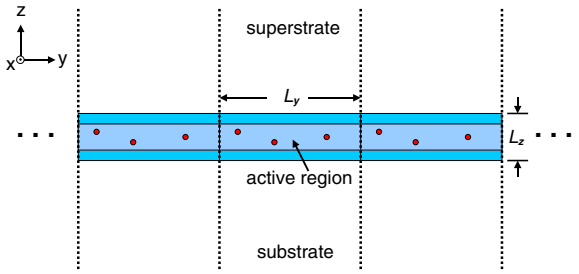

Fig. 1. A schematic illustration of the laterally repeating supercell geometry used in our simulations. Note that the supercell also repeats in the x-direction with periodicity of L_x (not drawn). The example shown in this figure illustrates a quantum well containing several randomly place dopant impurities.

semi-infinite superstrate and substrate regions described by constant potential and effective masses. The active region constitutes an $L_x \times L_y \times L_z$ finite computational domain over which solutions to the EMA equation is sought. Fig. 1 illustrates the specific example of the supercell geometry used to model a GaAs/AlGaAs QWIP: the active region of the supercell consists of the GaAs quantum well and surrounding AlGaAs barriers, and the semi-infinite superstrate and substrate regions consisting of the AlGaAs barrier material under flat-band condition. The quantum well region may contain a number of dopant impurity atoms.

The system is described by a one-band effective mass Hamiltonian with an energy-dependent anisotropic effective mass used to model the non-parabolic conduction band dispersion of the Γ valley. Band structure effects on optical matrix elements are included perturbatively using a 14-band $k \cdot p$ method based formulation [3]. The effects of discrete dopant impurities are incorporated as screened Coulomb potentials, similar to the technique used in Ref. [4]. The finite computational domain is divided into fine slices (typically ~3 Å thick) along the growth direction. The potential is assumed to be constant along the z-direction over each thin slice; along the lateral (x and y) dimensions, the effective mass equation is treated in k-space via plane wave expansion. We find that with lateral supercell dimensions of several hundred Angstroms, an 11×11 or 13×13 plane wave basis typically yields satisfactory results with good numerical convergence. Reflection coefficients can be obtained by solving the EMA equation over the computational domain using an algorithm analogues to the rigorous coupled wave analysis (RCWA) method [5] for optical waves, coupled with a stabilized transfer matrix technique [6]. The system is solved subject to periodic boundary conditions in the lateral directions, and scattering boundary conditions along the growth direction at the interfaces between the active region and the superstrate/substrate. The energy levels of confined states are found via seeking the poles of the reflection coefficient spectrum for an incident wave generated at the interface between the superstrate and the active region. For simplicity, the Hartree potential due to doping electrons is calculated non-self-consistently by assuming a charge density which is uniform in the x–y plane, but distributed in the z-axis according to a Gaussian function centered at the middle of the quantum well with a spread comparable to the well width. In principle our method could be easily adapted for full self-consistency. The mathematical details of the theoretical method will be described elsewhere [7].

3. Modeling results

The theoretical method we developed applies to both quantum well and quantum dot based infrared detectors. We first report on discrete dopant effects in QWIP structures, and then in QDIP structures.

3.1. Quantum well infrared photodetectors

We first examine band structure and impurity effects on the absorption property of QWIPs using a structure taken from the literature [8], with a 54 Å GaAs quantum well embedded in $Al_{0.26}Ga_{0.74}As$ barriers. In Fig. 2 we illustrate the effect of dopants on the quantum well ground state energy using a simplified simulation geometry. For this calculation, we use only a single dopant per supercell, placed at different z-positions within the quantum well. We vary

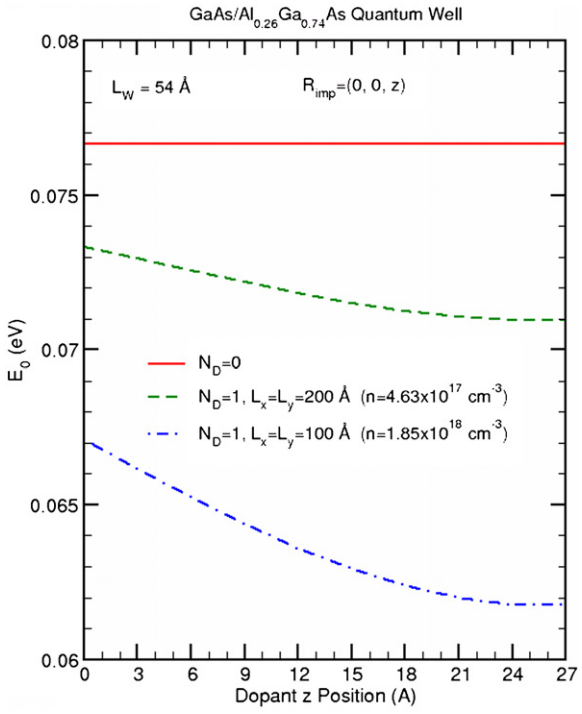

Fig. 2. Quantum well ground state energy as a function of dopant position. A single dopant is placed within a supercell. Two different lateral supercell sizes (100 Å × 100 Å and 200 Å × 200 Å, respectively corresponding to well doping levels of 4.6×10^{17} cm^{-3} and 1.9×10^{18} cm^{-3}). The $z = 0$ and $z = 27$ Å correspond to vertical dopant positions at the edge and center of the quantum well, respectively. The solid line indicates the ground state energy level when there are no dopants.

the nominal doping density by changing the supercell size. We note that the ground state energy is lowered as dopant density increases. The ground state energy is also lowered as the dopant moves from the edge of the quantum well to the center. In uniformly doped quantum wells, there would be a distribution of dopant locations along the growth direction in the well, which would result in level broadening.

We next examine dopant effects on optical properties. As we shall see, a dopant can modify or even induce additional optical transitions. To illustrate the origin of this phenomenon, we will use a simplified structure with a relatively small supercell (with 100 Å periodicity) containing only one dopant per supercell. Fig. 3 shows the lowest three energy levels in the reduced Brillouin zone of the lateral supercell as functions of the (lateral) wave vector along the x-direction, computed with and without the dopant. In Fig. 3 we see the first two conduction subbands, as well as a supercell zone-folded branch belonging to the first subband. For convenience, we refer to the non-folded first subband, the folded first subband, and the non-folded second subband respectively as b11, b12, and b21 (see Fig. 3). Note that the effect of the dopant is to lower the energy levels, as well as to induce a splitting at the zone boundary. We have also performed calculations using more dopants per supercell, and found that they lead to the further lowering of the energy levels (not shown).

The corresponding oscillator strengths as functions of lateral wave vector for the ground to the first and the second excited states are shown in Fig. 4. First we examine the results for the case with no dopants, for which we only have non-zero inter-subband (b11–b21) oscillator strength. The x-component (normal incidence) and the z-component (side-incidence) oscillator strengths are shown respectively in solid and dashed lines. We find that the oscillator strength for side-incidence light (z-component) is essentially independent of the wave vector. A simple one-band effective mass model would predict no normal incidence oscillator strength. Here we incorporated band structures effects perturbatively based on a 14-band $k \cdot p$ model [3], and find that the x-polarized (normal incidence) oscillator strength is zero at the zone center, but increases with k_x, reaching approximately 0.2% of that for the z-polarized light at $k_x = 0.02\ (2\pi/a)$. This is in general agreement with experimental results reported in the literature [8]. Note that the y-component is not present in this plot because the results shown are computed with $k_y = 0$; if we used non-zero k_y, we would also see non-zero y oscillator strengths.

When the dopant is introduced, the inter-subband oscillator strengths are largely unaffected. The only visible differences occur in the normal incidence (x-) component, at the zone boundary, where we find the dopant induced splitting between b11 and b12, and near the band-crossing point between b12 and b21. In addition, the y-component

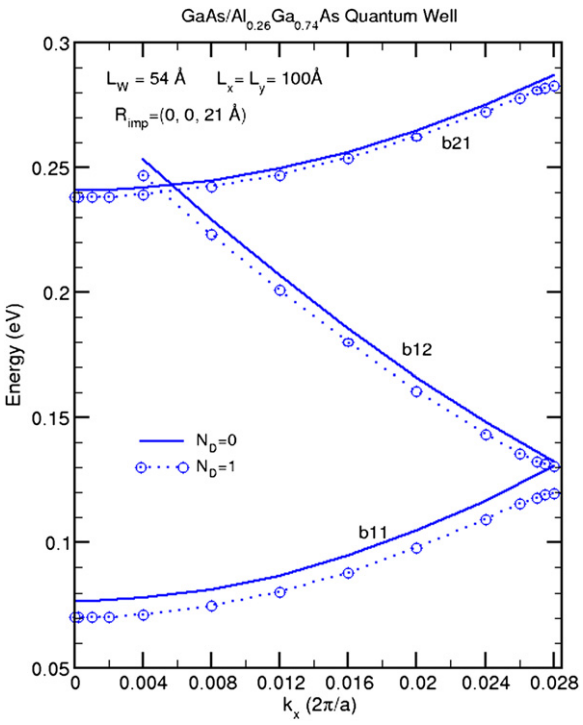

Fig. 3. The energy levels as functions of in-plane wave vector of the lowest three bound states of a quantum well computed with either no dopant ($N_D = 0$, indicated by the solid lines), or a single dopant ($N_D = 1$, indicated by open circles connected by dotted lines) in a 100 Å × 100 Å lateral supercell. The well width is 54 Å, and dopant is located at $z = 21$ Å (6 Å from the middle of the well).

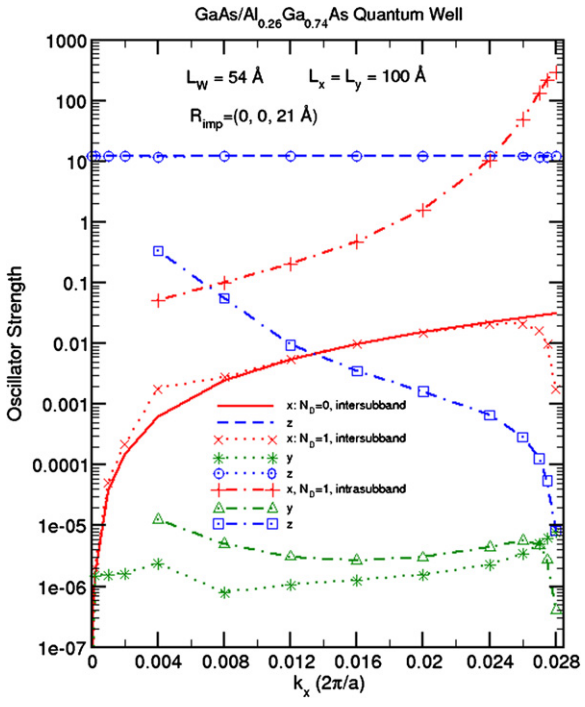

Fig. 4. Ground state to the first and the second excited states oscillator strengths as functions of in-plane wave vector. The simulations geometry is the same as that for Fig. 3. The results for the case with impurity scattering are shown in discrete symbols, and the results for the case without impurity scattering are shown as solid and dashed lines. The inter-subband transition results are given for both cases. Intra-subband transition results are given only for the case with impurity.

is now visible, but still considerable weaker than the x-component. The major difference introduced by the dopant is in the intra-subband absorption. Without the dopant potential, there would be no intra-subband optical transitions (in this case, between b11 and b12, the two branches of the first subband). However, as we can see in Fig. 4, the presence of the dopant can induce substantial normal incidence oscillator strength between these two branches, demonstrating the phenomenon of "dopant assisted intra-subband optical transition." In general, we observe that the dopant induced b11–b12$x(z)$ oscillator strength increases (decreases) with increasing k_x, and with decreasing transition energy. The intra-subband oscillator strength increases with k_x in part because of the transition energy (the energy denominator in the expression for oscillator strength) decreases with k_x. In fact, at the zone boundary it is even larger than the inter-subband z oscillator strength. While this large oscillator strength can lead to large normal incidence absorption coefficient in the long wavelength, it does not lead to significant photocurrent since the upper state (b12) in the optical transition is still deeply bound in the quantum well, and electrons photo-excited to this state can not escape into the AlGaAs barrier/transport region. We note that in general, while the strongest inter-subband transition is associated with side-incidence (z-polarized) light, the strongest intra-subband transitions are associated with normal incidence (x, y-polarized) light.

While the simplified example is useful in helping us understand the physical mechanisms involved in how dopant impurities can modify the optical properties of QWIPs, it is highly artificial in that the dopants are distributed in an ordered 2D array with the lateral periodicity of the supercell; the inter-dopant distances are always the same. In Fig. 5 we show the results of a more realistic simulation using a larger supercell with multiple dopants randomly placed in the quantum well region. In this case, we use 10 discrete donors in a 300 Å × 300 Å lateral supercell. We assume that the lowest five states are filled, and plot the oscillator strengths associated with transitions from these states to the higher states. For the energy range of interest shown in Fig. 5, we find that without discrete dopant effects, the only significant contribution is the z oscillator strength at a single transition energy (from the first to the second subband; inter-subband); the x and y oscillator strengths (non-zero due to band structure effects) are too small to be seen on this scale. When discrete dopant effects are included, we see a set of z oscillator strengths scattered about near the unperturbed transition energy, indicating level broadening. The transition energy with the highest z oscillator strength is slightly blue shifted from the no-dopant case. This is because the dopant induced energy lowering is larger in the lower subband than in the upper (as can be seen in Fig. 3). We also observe that x, y oscillator strengths (associated with normal incidence radiation) increase as the transition energy decreases. We attribute these x, y oscillator strengths to dopant assisted intra-subband optical transition, and expect them to result in strong

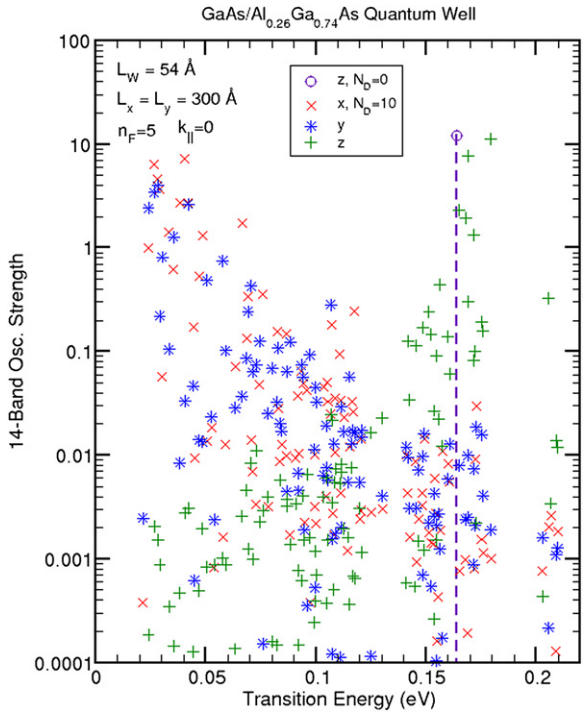

Fig. 5. Oscillator strengths as functions of transition energy in a GaAs/AlGaAs quantum well. The simulation geometry consists of a 300 Å × 300 Å lateral supercell containing a 54 Å quantum well, with 10 dopants placed randomly within the quantum well region in each supercell, and the lowest five states are assumed to be occupied. Oscillator strengths associated with filled states (lowest five states) to empty states are shown. For comparison, the circle with the dotted drop line indicates the z-component oscillator strength computed for a quantum well with no discrete dopant effects. A zero in-plane wave vector is used.

normal incidence absorption in the long wavelength. However, as pointed out in the discussions in Fig. 4 earlier, they are not expected to produce large photocurrents, since typically the upper states involved in these low energy transitions are considerable below the barrier of the quantum well (see Figs. 3 and 4), and electrons photo-excited to these states would not be able to escape out of the well.

3.2. Quantum dot infrared photodetectors

In this section we model the optical properties of a pyramid-shaped, square-base InAs/GaAs quantum dot. In the quantum dot being studied the base width is more than 10 times larger than the dot height. The structure is taken from the literature [9]. The dot height to base width ratio is kept low to reflect the dot geometry typically seen in present day QDIPs. The ground state is s-like as usual. Since the dot is x–y symmetric, the first excited states are the doubly-degenerate p_x-like and p_y-like states; due to the low-aspect-ratio, the p_z-like state is much higher in energy, and is typically unbound. By symmetry, the ground state to the p_x-like and p_y-like states transitions respectively have strong x and y oscillator strengths (normal incidence), but very little z oscillator strength. However, as mentioned

previously, such transitions do not generate significant photocurrent since the upper level is too low in energy for the photo-excited electrons to escape from the dot potential with significant probability. The next set of excited states is d-like. By symmetry, the z-component of the oscillator strength dominates (x and y oscillator strengths are strictly zero if band structure effects are not taken into account). However, this symmetry can be broken easily if discrete dopant effects are taken into account. This is apparent when we consider the fact that the size of the hydrogenic radius associated with a typical dopant wave function is comparable to the dot dimensions.

Fig. 6 shows the energy levels in a low-aspect-ratio quantum dot with base width of 265 Å and dot height of 25 Å, resting on a 5 Å thick wetting layer. The calculation includes the potential from the single discrete dopant, placed at several positions with common x, y coordinates but different z coordinates. With respect to the quantum dot, the dopant is centered along the y-direction and off-center along the x-direction. The dopant is purposely placed off-center laterally to destroy the symmetry along the x-direction (in-plane). At the same time, it is also located fairly close to the center in order to produce a sufficiently large perturbation on the quantum dot wave function. This asymmetry is reflected in the calculated energy levels. For instance, the splitting between the p_x-like and p_y-like states is quite apparent. The oscillator strengths associated with the transitions from the ground state to the three d-like states are shown in Fig. 7. Without the dopant potential, the z-component of the oscillator strength dominates, even when band structure effects are taken into account. However, when the dopant potential is taken into consideration, the x-component of the oscillator strength can become even stronger than the z-component if the dopant is located in a position where it can cause substantial disturbance in the quantum dot wave function. We take a specific dopant z location (one which produced the largest x oscillator strength) and plots the oscillator strength components against transition energy in Fig. 8. The s-like state to p_x-like and p_y-like states transitions (not shown in Fig. 7) respectively produce strong x- and y-component (normal incidence) oscillator strengths, which, as mentioned earlier, do not produce significant photocurrents. The oscillator strengths associated with transitions from the s-like state to the three d-like states (which we label d1, d2, and d3) are also shown (these are also plotted in Fig. 7, at $z = 40$ Å). Without the dopant potential, the lowest d-like state (d1) is odd in both x and y, and the next two d-like states (d2 and $d3$) are even in both x and y. The s–d1 transition produces no oscillator strengths, and the s–d2 and s–d3 transitions produce only z oscillator strengths.

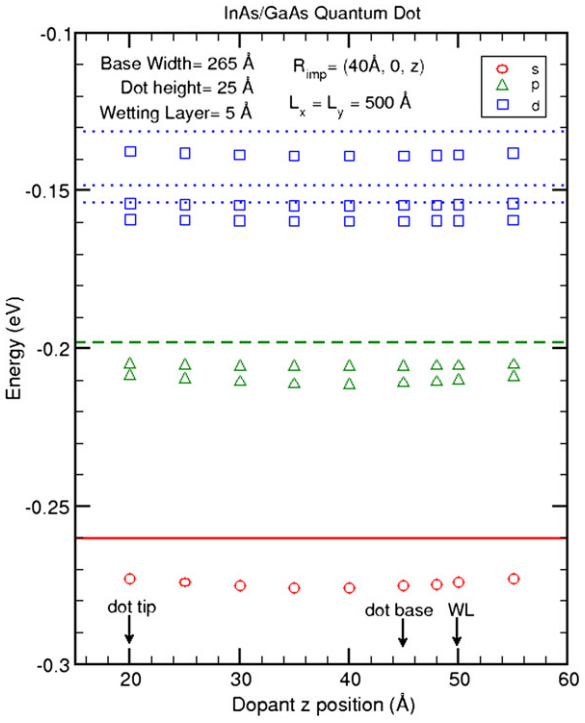

Fig. 6. Low lying quantum dot energy levels (indicated by discrete symbols) as functions of dopant position along the z-direction. A supercell with lateral dimensions of 500 Å × 500 Å is used for the calculation. Centered in each supercell is a single pyramidal InAs quantum dot with base dimensions of 265 Å × 265 Å and height of 25 Å, resting on top of a 5 Å InAs wetting layer, and embedded in a GaAs matrix. A single dopant is located at (40 Å, 0, z), i.e., off-center along the x-direction, with varying z-position. The solid, dashed, and dotted lines respectively indicate the s-, p-, and d-like state energy levels computed without the dopant potential.

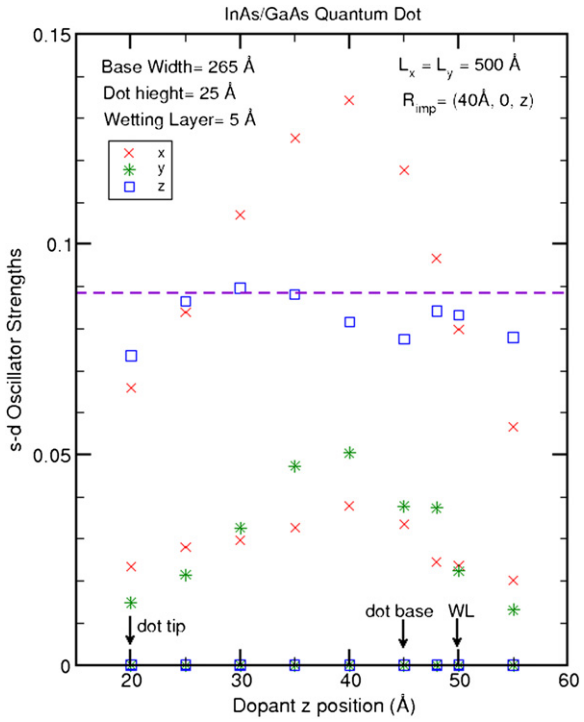

Fig. 7. Oscillator strengths associated with the transitions from the ground state to the second set of excited states (d-like) for the same dot geometry and dopant positions as described in Fig. 6. The dashed lines indicate the z-component (x and y components are insignificant) oscillator strength computed without the dopant potential.

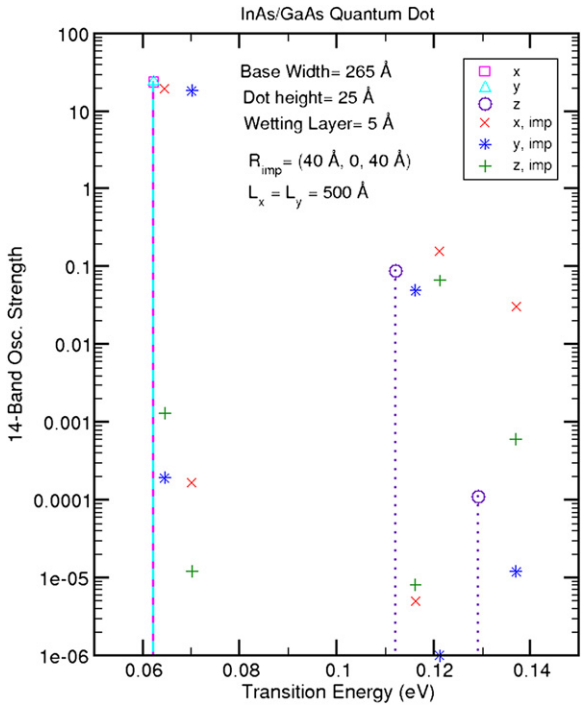

Fig. 8. Oscillator strengths as functions of transition energy associated with the transitions from the ground state to the first set of excited states (the p_x-like and p_y-like), and to the second set of excited states (d-like) for the same dot geometry as described in Fig. 6. The dopant is located 40 Å off-center along the x-direction, and 5 Å above the dot base along the z-direction. The oscillator strengths are indicated by discrete symbols. For comparison, we also include oscillator strengths computed without including dopant effects; the results are indicated by symbols with drop lines.

When the dopant potential is taken into consideration, all three of the s–d transitions can produce significant normal incidence (x or y) oscillator strengths. We should be point out, however, that Fig. 8 illustrates the case where the dopant potential is optimally located to produce very strong perturbations on the quantum dot wave function. If the dopant is outside the quantum dot, then its effect on the quantum dot optical property is minimal.

4. Summary and discussion

We conducted theoretical studies on the influence of band structure effects and discrete dopant effects on intersubband optical transitions in quantum wells and quantum dots. For both quantum wells and quantum dots, we find that although band structure effects could introduce nonzero normal incidence oscillator strengths in cases where simple one-band effective mass model would not, the effect tends to be small. Discrete dopant effects tend to be more noticeable in heavily doped quantum wells, and in quantum dots where dopants are strategically placed.

In quantum wells, discrete dopant effects can induce long wavelength infrared absorption through impurity assisted intra-subband optical transitions. The resulting intra-subband absorption tends to occur at lower transitions energies than the intended inter-subband absorption. In QWIP measurements, long wavelength absorption typically appears as an increasing baseline in the infrared spectrum, and is attributed to free carrier absorption in the contact layers. Our results indicate that in a heavily doped QWIP structure, dopant induced intra-subband absorption could also contribute to this long wavelength infrared absorption.

In QDIPs, we find that a dopant atom placed off-center and inside a quantum dot can easily destroy the symmetry and modify the selection rule. We showed that when dopant effects are included, the x and y-components of the oscillator strength associated with the s-like state to the three d-like states transitions could become even stronger than the z-component, even though the oscillator strength should be dominated by the z-component when the dopant potential is absent. This could provide a partial explanation to the normal incidence absorption observed in a low-aspect-ratio quantum dots, although other explanations, such as transitions to even higher states or finite cavity edge effects [10], are also possible.

Acknowledgments

We are grateful to E. Blazejewski and RT. Odle for their encouragement and support. The research described in this paper was carried out in part at the Jet Propulsion Laboratory, California Institute of Technology, through an agreement with the National Aeronautics and Space Administration.

References

[1] J. Phillips, J. Appl. Phys. 91 (2002) 4590.
[2] V. Ryzhii, I. Khmyrova, M. Ryzhii, V. Mitin, Semicond. Sci. Technol. 19 (2004) 8.
[3] C.W. Cheah, L.S. Tan, G. Karunasiri, J. Appl. Phys. 91 (2002) 5105.
[4] G.D. Sanders, Y.-C. Chang, Phys. Rev. B 35 (1987) 1300.
[5] M.G. Moharam, Eric B. Grann, Drew A. Pommet, T.K. Gaylord, J. Opt. Soc. Am. A 12 (1995) 1068.
[6] M.G. Moharam, Drew A. Pommet, Eric B. Grann, T.K. Gaylord, J. Opt. Soc. Am. A 12 (1995) 1077.
[7] Y.C. Chang, D.Z.-Y. Ting, unpublished.
[8] H.C. Liu, M. Buchanan, Z.R. Wasilewski, Appl. Phys. Lett. 72 (1998) 1682.
[9] P. Boucaud, S. Sauvage, C.R. Physique 4 (2003) 1133.
[10] K.K. Choi, K.L. Bacher, Y. Wu, Electrochem. Soc. Proc. 98-21 (1998) 71.